Excitation-Gap Scaling near Quantum Critical Three-Dimensional Antiferromagnets

M. Lohöfer and S. Wessel*

Institut für Theoretische Festkörperphysik, JARA-FIT and JARA-HPC, RWTH Aachen University, 52056 Aachen, Germany

(Received 17 October 2016; revised manuscript received 15 December 2016; published 6 April 2017)

By means of large-scale quantum Monte Carlo simulations, we examine the quantum critical scaling of the magnetic excitation gap (the triplon gap) in a three-dimensional dimerized quantum antiferromagnet, the bicubic lattice, and identify characteristic multiplicative logarithmic scaling corrections atop the leading mean-field behavior. These findings are in accord with field-theoretical predictions that are based on an effective description of the quantum critical system in terms of an asymptotically free field theory, which exhibits a logarithmic decay of the renormalized interaction strength upon approaching the quantum critical point. Furthermore, using bond-based singlet spectroscopy, we identify the amplitude (Higgs) mode resonance within the antiferromagnetic region. We find a Higgs mass scaling in accord with field-theoretical predictions that relate it by a factor of $\sqrt{2}$ to the corresponding triplon gap in the quantum disordered regime. In contrast to the situation in lower-dimensional systems, we observe in this three-dimensional coupled-dimer system a distinct signal from the amplitude mode also in the dynamical spin structure factor. Its width is observed to vanish proportional to the Higgs mass in the accessible proximity to the quantum critical point.

DOI: 10.1103/PhysRevLett.118.147206

Quantum critical three-dimensional antiferromagnets provide considerably valuable condensed matter realizations of (infrared) asymptotically free quantum field theories: based on the quantum-to-classical mapping, the critical field theory that describes the underlying quantum critical point is the classical four-dimensional O(3) ϕ^4 theory [1–6]. Because of a logarithmic decay of the renormalized interaction strength upon approaching the critical point, this field theory exhibits logarithmic corrections to a Gaussian fixed point [7–10]. This leads to characteristic multiplicative logarithmic scaling corrections to the bare mean-field behavior in various physical quantities that are in principle accessible by several experimental probes, such as in thermodynamic measurements or neutron and light scattering techniques [6,11–14], if probed at the relevant energy scales near the quantum critical point.

A well characterized example system of this scenario is provided by the dimerized spin-half compound $TlCuCl_3$: under the application of hydrostatic pressure, this system features a quantum phase transition from a gapped quantum disordered state into an antiferromagnetically ordered phase [15]. The magnetic excitations across the quantum critical region have been analyzed in detail recently by inelastic neutron scattering [16–18]. These studies identified the evolution of the gapped magnon mode from the dimerized quantum disordered regime (frequently referred to also as the "triplon" mode in reference to its threefold degeneracy in the isotropic Heisenberg spin-exchange case), to the low-energy (transverse) Goldstone modes that accompany the spontaneous breaking of spin-rotation symmetry in the ordered phase. Furthermore, inelastic neutron scattering on this compound also identified a gapped (longitudinal) amplitude mode of the order-parameter field [17,18], frequently referred to recently as a Higgs mode [19,20]. This amplitude mode softens upon approaching the quantum critical point [21,22]. Within a Gaussian field theory description, its excitation gap (the Higgs mass) $\Delta_H(g)$ scales as $\Delta_H(g) = \sqrt{2}\Delta(g)$ with the mass scale $\Delta(g)$ in the vicinity of the quantum critical point [6,23]. Here, g is a dimensionless tuning parameter (related to pressure), with the critical point located at $g = g_c$. The mass scale $\Delta(g)$ in the antiferromagnetic region, $g < g_c$, relates via $\Delta(g) = \Delta_t[g_c + (g_c - g)]$ to the triplon excitation gap $\Delta_t(g)$ in the quantum disordered regime, $g > g_c$. Recently, the data for $TlCuCl_3$ have been reanalyzed from the perspective of the asymptotic freedom scenario [6]. It was, however, also argued that the available experimental data may not provide robust evidence for logarithmic corrections, given the size of the error margin and a reduced number of data points near the quantum critical point [14]. In order to probe for logarithmic scaling corrections in quantum critical spin dimer systems, it is thus crucial to compare these field-theoretical predictions with unbiased high-precision results.

Here, we provide such a characterisation of the quantum critical scaling of the excitations in three-dimensional dimerized antiferromagnets by addressing, directly, the relevant dynamical quantities using quantum Monte Carlo (QMC) simulations. In particular, we analyze the scaling of the magnetic (triplon) excitation gap (Δ_t) as well as the Higgs mass (Δ_H) near the quantum critical bicube Heisenberg model, the most basic three-dimensional coupled dimer system. By probing the system in close vicinity to its quantum critical point, we identify

multiplicative logarithmic scaling corrections and also confirm the characteristic $\sqrt{2}$ value of the gap ratio. Furthermore, we find that—in contrast to the two-dimensional case of the Heisenberg bilayer system—the Higgs excitation mode in the three-dimensional bicube system can be identified not only by the singlet-based scalar susceptibility [19,24–26] but also as a distinct resonance mode in the dynamical spin structure factor, which relates directly to inelastic neutron scattering.

Before presenting our findings, we first introduce the model system and the used QMC approach. The spin-1/2 Heisenberg model on the bicubic lattice consists of an arrangement of spin dimers on a simple cubic lattice: each unit cell contains one such dimer, with a common vector connecting the two spins forming the dimer in each unit cell [14,27]. The Hamiltonian is hence given by

$$H = J' \sum_i \mathbf{S}_{i1} \cdot \mathbf{S}_{i2} + J \sum_{\langle i,j \rangle} (\mathbf{S}_{i1} \cdot \mathbf{S}_{j1} + \mathbf{S}_{i2} \cdot \mathbf{S}_{j2}), \quad (1)$$

where spin $\mathbf{S}_{i\mu}$ resides on the first ($\mu = 1$) and second ($\mu = 2$) site of the dimer within the ith unit cell of the cubic lattice (see Fig. 1 for an illustration). Furthermore, J' denotes the coupling within each dimer, and J the coupling between spins in different unit cells. In the following,

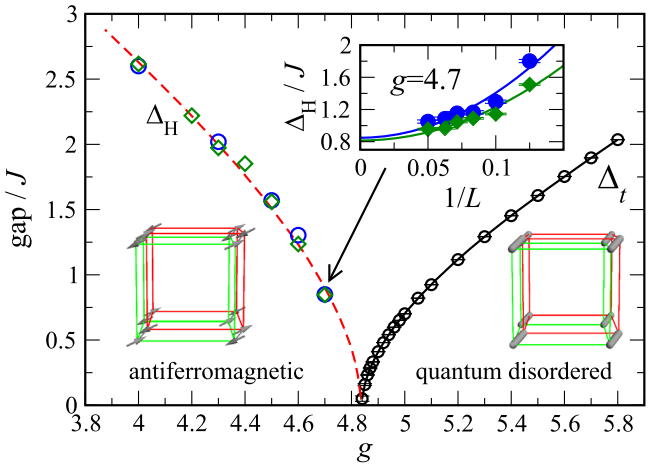

FIG. 1. Triplon (Δ_t) and Higgs (Δ_H) gap in the vicinity of the quantum critical point of the bicube coupled dimer antiferromagnet. The dashed line indicates a scaling of $\Delta_H(g) = \sqrt{2}\Delta_t[g_c + (g_c - g)]$. Estimates for $\Delta_H(g < g_c)$ from the dynamical spin (singlet) structure factor are shown by circles (diamonds), with an estimated uncertainty of order the symbol size. The results for $\Delta_t(g > g_c)$ are shown by circles, and the full line is a guide to the eye. The upper inset shows, by circles, (diamonds) the finite-size values of Δ_H as estimated from the position of the second (main) peak in $S_S(\omega, 0)$ ($S_B(\omega, \mathbf{Q})$) at $g = 4.7$. Solid lines show extrapolations linear in $1/L^2$ to the thermodynamic limit. Both phases on the bicube lattice are illustrated by the lower insets, where colored (grey) bonds denote J (J') couplings.

we denote by $g = J'/J$ the ratio of the two coupling constants and set the lattice constant a of the cubic lattice to 1. For this spin dimer system, multiplicative logarithmic corrections were identified in several thermodynamic quantities, such as the g dependence of the ordering temperature, in the vicinity of the quantum critical point at $g = g_c = 4.837\,04(6)$ [14] that separates the antiferromagnetic low-g phase from the quantum disordered large-g regime. The bicube model contains an inversion symmetry with respect to exchanging the spins with $\mu = 1, 2$ in all unit cells. We account for this additional quantum number by assigning a forth component to an originally three-dimensional momentum space vector. Hence, $\mathbf{k} = (k_x, k_y, k_z, k_p)$, with $k_p = 0$ or π, denoting the symmetric and antisymmetric channel with respect to dimer inversion, respectively. Correspondingly, each spin is assigned a position vector $\mathbf{r}_{i\mu}$, with a forth component equal to 0 (1), for $\mu = 1$ ($\mu = 2$).

Of particular interest to our analysis is the dynamical spin structure factor $S_S(\omega, \mathbf{k}) = (1/N_s) \times \int dt \sum_{i,j,\mu,\nu} e^{i(\omega t - \mathbf{k}\cdot(\mathbf{r}_{i\mu} - \mathbf{r}_{j\nu}))} \langle \mathbf{S}_{i\mu}(t) \cdot \mathbf{S}_{j\nu}(0) \rangle$, where N_s denotes the number of spins, and $k_p = 0$ ($k_p = \pi$) refers to the symmetric (antisymmetric) sector. In the presence of long-range antiferromagnetic order, one may also distinguish the components of $S_S(\omega, \mathbf{k})$ parallel and transverse to the order parameter orientation, in which case $S_S(\omega, \mathbf{k})$ represents a rotational average that is probed by the QMC simulations. In addition to the spin correlations, we also analyze correlations among the dimer bond-based spin-exchange terms, $B_i = \mathbf{S}_{i1} \cdot \mathbf{S}_{i2}$, and define a corresponding scalar response function in terms of the dynamical singlet structure factor $S_B(\omega, \mathbf{k}) = (1/N_d) \int dt \sum_{i,j} e^{i(\omega t - \mathbf{k}\cdot(\mathbf{r}_i - \mathbf{r}_j))} \langle B_i(t) B_j(0) \rangle$, where $N_d = N_s/2$ denotes the number of dimers. Here, $\mathbf{k}$ and the $\mathbf{r}_i$ denote three-dimensional cubic lattice k-space and lattice position vectors (i.e., with a vanishing forth component), respectively, where the operator B_i resides at position $\mathbf{r}_i$ on the simple cubic lattice.

We analyze these dynamical quantities of the bicube Heisenberg model using QMC simulations based on the stochastic series expansion method with directed loop updates [28–30], considering finite systems with $N_s = 2L^3$ lattice sites and periodic boundary conditions. We used systems with L ranging from 8 up to 26 close to the quantum critical point, which corresponds to up to $N_s = 35\,152$ spins. In order to access ground state properties, the inverse temperature β has been chosen to be sufficiently large. This typically required $\beta J \geq 2L$. In order to calculate the dynamical spin structure factor, we efficiently [31] measured the imaginary-time displaced spin-spin correlation functions directly in Matsubara frequency representation [32]. The numerical inversion to obtain $S_S(\omega, \mathbf{k})$ from the Matsubara frequency QMC data was performed using the stochastic analytic continuation method in the formulation of Ref. [35]. For the dynamical singlet structure

factor $S_B(\omega, \mathbf{k})$, we measured the corresponding bond-bond correlation functions directly in imaginary time, binned over finite-width imaginary-time windows [31]. Using an appropriate kernel for the analytic continuation, we can directly relate $S_B(\omega, \mathbf{k})$ to these imaginary-time binned data [26].

The dynamical spin structure factor $S_S(\mathbf{k}, \omega)$ is dominated by the single-magnon dispersion, which for $g < g_c$ softens at the antiferromagnetic Bragg peak position $\mathbf{Q} = (\pi, \pi, \pi, \pi)$, while a finite triplon gap Δ_t exists at $\mathbf{k} = \mathbf{Q}$ in the structure factor data for $g > g_c$ [32]. For a quantitative analysis of the g dependence of Δ_t in the thermodynamic limit, we performed a systematic finite-size scaling analysis. For this purpose, we obtained the values of Δ_t for various $g > g_c$ and different system sizes by extracting from the imaginary-time spin-spin correlation function $S_S(\tau, \mathbf{k})$ at $\mathbf{k} = \mathbf{Q}$ the low-temperature asymptotic form $S_S(\tau, \mathbf{Q}) \propto \exp(-\tau\Delta_t)$. Here, $S_S(\tau, \mathbf{k})$ is obtained from the Matsubara frequency data by a discrete Fourier back-transformation [36]. Based on the finite-size dependence $\xi_\tau(L) = \xi_\tau - b\exp(cL)$ of the correlation-length in the imaginary-time direction, where $\xi_\tau = 1/\Delta_t$ [32,37], and b and c are fit parameters, we obtain the thermodynamic limit values of Δ_t (cf. Fig. 1).

In order to closer examine the quantum critical scaling, Δ_t is shown as a function of the relative distance from the quantum critical point, $(g - g_c)/g_c$, in Fig. 2 in a log-log plot. Also included in Fig. 2 is a comparison of the data to a square-root scaling proportional to $(g - g_c)^{1/2}$, corresponding to Gaussian mean-field behavior. It is clear from Fig. 2, that this form does not account for the gap data scaling. In fact, the logarithmic decay of the renormalized interaction strength upon approaching the quantum critical point leads to a logarithmic correction to the mean-field scaling behavior,

$$\Delta_t(g) \propto \left(\frac{g - g_c}{g_c}\right)^{1/2} \left|\ln\frac{g - g_c}{g_c}\right|^{-5/22}, \qquad (2)$$

in the vicinity of the quantum critical point [6,10,38,39]. This follows from the quantum-to-classical mapping with a dynamical critical exponent $z = 1$, and relating $\Delta_t = \xi_\tau^{-1}$ to the correlation length in the imaginary-time direction. The solid line in Fig. 2 shows that the numerical data are well in accord with this analytic prediction up to values $(g - g_c)/g_c \lesssim 0.3$. Fitting the numerical data to the scaling law in Eq. (2) with the exponent $5/22$ replaced by a free fit parameter $\bar{\nu}$, we obtain an independent estimate of $\bar{\nu} = 5.2(1)/22$, when all data with $(g - g_c)/g_c < 0.25$ is included, and with a reduced χ^2 value (per degree of freedom) of $\chi^2/\mathrm{DOF} = 1.2$. Further analysis shows that the triplon gap data does not fit well to such a scaling form anymore (with values of χ^2/DOF rapidly exceeding values of order 10), if further data points beyond $(g - g_c)/g_c > 0.35$ are included into the fit range. Also shown in Fig. 2 is the large-g perturbative expansion result $\Delta_t = J' - 3J + O(J^2)$ for the triplon gap, which traces the data well for $(g - g_c)/g_c > 1$. We note that in the crossover region no indication for a distinct pure Gaussian mean-field behavior can be seen.

We next address the amplitude (Higgs) mode in the bicube model. Figure 3 shows the spin spectral function $S_S(\omega, \mathbf{Q})$ for various values of $g < g_c$. While the signal is dominated by the Bragg peak at $\omega = 0$, we also identify a second, distinct spectral feature for all shown values of g. This broader peak furthermore softens upon approaching the quantum critical point and also sharpens closer to g_c. By tracing the peak position as a function of g, we obtain the excitation energies indicated by open circles in Fig. 1, after performing, again, an extrapolation to the thermodynamic limit (an example of which is shown in the inset of Fig. 1

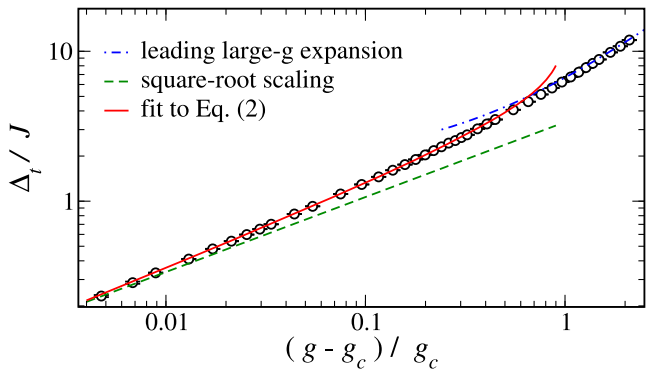

FIG. 2. Quantum critical scaling of the triplon excitation gap Δ_t in the vicinity of the quantum critical point. The QMC estimates, obtained after a finite-size extrapolation, are shown by black circles. The solid line is a fit to Eq. (2) of the data with $(g - g_c)/g_c < 0.3$, the dashed line indicates Gaussian theory square-root scaling, and the dashed-dotted line the leading large-g perturbative expansion result.

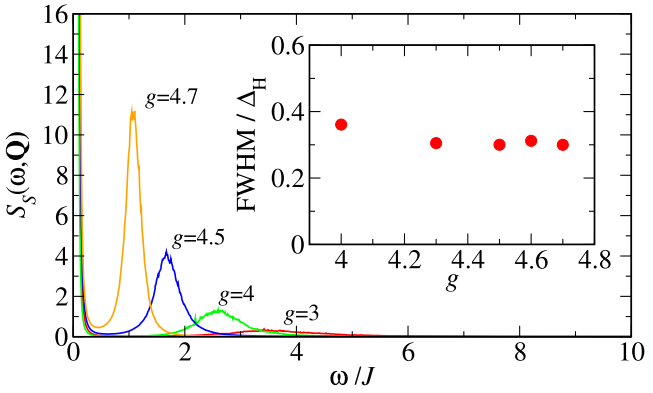

FIG. 3. Dynamical spin structure factor $S_S(\omega, \mathbf{Q})$ at the ordering wave vector for different values of the coupling ratio g, as obtained from QMC simulations with $L = 20$, $\beta = 40/J$. The inset shows the ratio between the width (FWHM) and the position Δ_H of the second peak, where the estimated uncertainty is of order the symbol size.

for $g = 4.7$). Also included in Fig. 1 is the field-theory prediction [6,23] for the Higgs mass scaling $\Delta_H(g) = \sqrt{2}\Delta(g)$, with $\Delta(g) = \Delta_t[g_c + (g_c - g)]$. The extrapolated peak positions closely follow this scaling prediction, indicating that this second feature in $S_S(\omega, \mathbf{Q})$ indeed signals the amplitude mode of the bicube system. One may compare this to the case of the two-dimensional bilayer model, where the amplitude mode's contribution to the spin spectral function is masked by a broader tail atop the Goldstone mode [19,26,40]. Here, in the three-dimensional bicube system, we can clearly identify the amplitude mode in the dynamical spin structure factor. This observation is well in accord with the identification of a broad amplitude mode and its softening near criticality in the neutron scattering data [17,18] on $TlCuCl_3$.

We can access the amplitude mode also from the dynamical singlet structure factor $S_B(\omega, 0)$. Because of its scalar character, this quantity contains the amplitude-mode signal without being masked by the low-energy Goldstone modes [19,24–26]. This fact was employed in Ref. [26] in order to access the amplitude mode for the two-dimensional bilayer system. Here, we perform an analysis of $S_B(\omega, 0)$ for the bicube model: Figure 4 shows $S_B(\omega, 0)$ for various values of g. The amplitude mode dominates $S_B(\omega, 0)$ as a pronounced low-energy peak that softens upon approaching the quantum critical point. It is followed by a second, broader peak at more elevated energies of $\omega/J \approx 7.5$, which exhibits no such clear g dependence, and thus does not relate to the critical low-energy spectrum. From an extrapolation of the main peak's position to the thermodynamic limit, we extract the Higgs mass scaling in the vicinity of the quantum critical point (this extrapolation is also shown explicitly for $g = 4.7$ in the inset of Fig. 1). The resulting g dependence of the Higgs mass Δ_g is shown in the main panel of Fig. 1. We find that the extrapolated

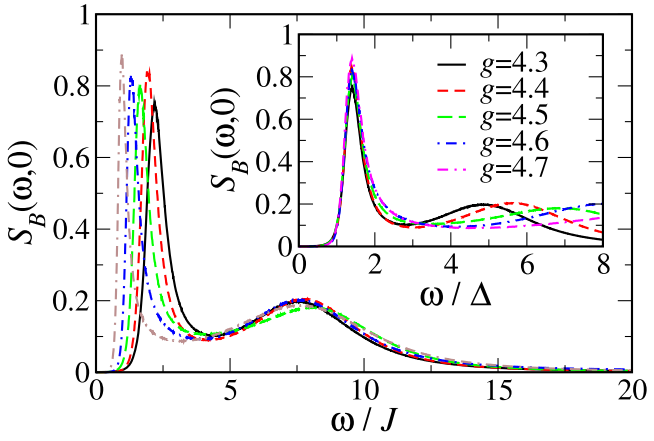

FIG. 4. Dynamical singlet structure factor $S_B(\omega, 0)$ for different values of the coupling ratio g, as obtained from QMC simulations with $L = 16$, $\beta = 32/J$. The inset shows a collapse of the Higgs peak after rescaling of the ω axis by the energy scale $\Delta = \Delta_H/\sqrt{2}$.

values of the main peak positions in $S_B(\omega, 0)$ agree remarkably well with the extrapolated values for Δ_H obtained from $S_S(\omega, \mathbf{Q})$. Hence, both the low-energy peak in $S_B(\omega, 0)$ as well as the finite energy peak in $S_S(\omega, \mathbf{Q})$ relate to the amplitude mode in the bicube system, with an excitation energy that (i) softens upon approaching the quantum critical point and (ii) exhibits a g dependence in accord with the field-theory prediction, $\Delta_H = \sqrt{2}\Delta$ [6,23].

Even though the line shape of the Higgs peak is affected by the analytical continuation procedure, our numerical results for the overall form of the Higgs peak compare well to the low-energy scaling form $S_B(\omega, 0) = \Delta^{d+z-2/\nu}\Phi(\omega/\Delta)$ of the scalar response function [41,42]. Indeed, at the mean-field level with $\nu = 1/2$, and for $d + z = 3 + 1$, this simplifies to $S_B(\omega, 0) = \Phi(\omega/\Delta)$, which is in good accord with the overall collapse of the Higgs peak signals shown in the inset of Fig. 4, in particular in the low-ω section. This furthermore shows that the Higgs peak sharpens upon approaching g_c, with an only weakly g-dependent ratio R between its width and the Higgs mass. Within the accuracy that is available through the analytic continuation scheme, we estimate this ratio from the inset of Fig. 4 in terms of its full width at half maximum (FWHM), to $R = 0.4(1)$. A roughly constant ratio between the FWHM and the Higgs mass is also obtained for the Higgs peak signal in the dynamical spin structure factor, cf. the inset of Fig. 3. An approximately constant width-to-gap ratio was also observed for $TlCuCl_3$ [17,18] and obtained within mean-field theory calculations [4]. On the other hand, logarithmic corrections due to fluctuations were shown in renormalization group calculations [42] to eventually reduce the width-to-gap ratio towards zero upon approaching g_c in three-dimensional quantum critical systems [21]. To observe this critical reduction in the Higgs peak width for the bicube model, and to provide comparable accuracy on the width as we obtained here for the excitation gap, would require high-statistics simulations closer to g_c than those accessible here.

In summary, we presented robust evidence for logarithmic corrections to the leading mean-field scaling of the triplon excitation gap softening near the quantum critical point. We observed a distinct signal of the amplitude mode in the spin and singlet spectral functions. This mode furthermore softens and sharpens upon approaching the quantum critical point, with an excitation gap that scales consistently with a $\sqrt{2}$ ratio to the corresponding triplon excitation energy. These findings close the gap between the field-theoretical description of fundamental quantum phase transitions and their experimental investigation in three-dimensional dimerized antiferromagnets. Within the accessed parameter region close to criticality, the width of the Higgs peak scales essentially proportional to its mass. Future work may aim at identifying the logarithmic reduction in the critical width-to-gap scaling of the Higgs peak to a similar precision as provided here for the excitation gaps,

as well as consider thermal effects on the amplitude mode and its dispersion relation in a similar quantitative form.

We thank F. Mila and K. P. Schmidt for discussions, Z. Y. Meng for mentioning related findings [43], the Deutsche Forschungsgemeinschaft (DFG) for support under Grant No. FOR 1807, and the IT Center at RWTH Aachen University and the JSC Jülich for access to computing time through JARA-HPC.

*wessel@physik.rwth-aachen.de

[1] S. Chakravarty, B. I. Halperin, and D. R. Nelson, Phys. Rev. Lett. **60**, 1057 (1988).
[2] S. Sachdev, in *Understanding Quantum Phase Transitions*, edited by L. D. Carr (Taylor & Francis, Boca Raton, 2010).
[3] S. Sachdev, *Quantum Phase Transitions* (Cambridge University Press, Cambridge, England, 2011).
[4] Y. Kulik and O. P. Sushkov, Phys. Rev. B **84**, 134418 (2011).
[5] J. Oitmaa, Y. Kulik, and O. P. Sushkov, Phys. Rev. B **85**, 144431 (2012).
[6] H. D. Scammell and O. P. Sushkov, Phys. Rev. B **92**, 220401 (2015).
[7] J. Zinn-Justin, *Quantum Field Theory and Critical Phenomena* (Oxford University Press, Oxford, 2002).
[8] R. Kenna and C. B. Lang, Nucl. Phys. **B393**, 461 (1993).
[9] R. Kenna and C. B. Lang, Nucl. Phys. **B411**, 340 (1994).
[10] R. Kenna, in *Order, Disorder and Criticality*, edited by Y. Holovatch (World Scientific, Singapore, 2013), Vol. 3, Chap 1.
[11] O. Nohadani, S. Wessel, and S. Haas, Phys. Rev. B **72**, 024440 (2005).
[12] M. Tsukamoto, C. Batista, and N. Kawakami, J. Magn. Magn. Mater. **310**, 1360 (2007).
[13] M. T. Kao and F. J. Jiang, Eur. Phys. J. B **86**, 419 (2013).
[14] Y. Q. Qin, B. Normand, A. W. Sandvik, and Z. Y. Meng, Phys. Rev. B **92**, 214401 (2015).
[15] Ch. Rüegg, A. Furrer, D. Sheptyakov, T. Strässle, K. W. Krämer, H.-U. Güdel, and L. Mélési, Phys. Rev. Lett. **93**, 257201 (2004).
[16] Ch. Rüegg, B. Normand, M. Matsumoto, Ch. Niedermayer, A. Furrer, K. W. Krämer, H.-U. Güdel, Ph. Bourges, Y. Sidis, and H. Mutka, Phys. Rev. Lett. **95**, 267201 (2005).
[17] Ch. Rüegg, B. Normand, M. Matsumoto, A. Furrer, D. F. McMorrow, K. W. Krämer, H.-U. Güdel, S. N. Gvasaliya, H. Mutka, and M. Boehm, Phys. Rev. Lett. **100**, 205701 (2008).
[18] P. Merchant, B. Normand, K. W. Krämer, M. Boehm, D. F. McMorrow, and Ch. Rüegg, Nat. Phys. **10**, 373 (2014).
[19] D. Podolsky, A. Auerbach, and D. P. Arovas, Phys. Rev. B **84**, 174522 (2011).
[20] D. Pekker and C. M. Varma, Annu. Rev. Condens. Matter Phys. **6**, 269 (2015).
[21] I. Affleck and G. F. Wellman, Phys. Rev. B **46**, 8934 (1992).
[22] S. Sachdev, Nat. Phys. **4**, 173 (2008).
[23] S. Sachdev, arXiv:0901.4103.
[24] M. Matsumoto, H. Kuroe, A. Oosawa, and R. Sekine, J. Phys. Soc. Jpn. **77**, 033702 (2008).
[25] M. Matsumoto, J. Phys. Soc. Jpn. **83**, 084704 (2014).
[26] M. Lohöfer, T. Coletta, D. G. Joshi, F. F. Assaad, M. Vojta, S. Wessel, and F. Mila, Phys. Rev. B **92**, 245137 (2015).
[27] S. Jin and A. W. Sandvik, Phys. Rev. B **85**, 020409(R) (2012).
[28] A. W. Sandvik, Phys. Rev. B **59**, R14157 (1999).
[29] O. F. Syljuasen and A. W. Sandvik, Phys. Rev. E **66**, 046701 (2002).
[30] F. Alet, S. Wessel, and M. Troyer, Phys. Rev. E **71**, 036706 (2005).
[31] F. Michel and H. G. Evertz, arXiv:0705.0799; F. Michael, Ph. D. Thesis, Univ. of Graz, 2007.
[32] See Supplemental Material at http://link.aps.org/supplemental/10.1103/PhysRevLett.118.147206 for scans of the dynamical spin structure factor through the Brillouin zone, further details on the measurement method, and the finite-size extrapolation of the triplon excitation gap, which includes Refs. [33] and [34].
[33] D. G. Joshi, K. Coester, K. P. Schmidt, and M. Vojta, Phys. Rev. B **91**, 094404 (2015).
[34] D. G. Joshi and M. Vojta, Phys. Rev. B **91**, 094405 (2015).
[35] K. S. D. Beach, arXiv:cond-mat/0403055.
[36] L. Pollet and N. V. Prokof'ev, Phys. Rev. Lett. **109**, 010401 (2012).
[37] M. Matsumoto, C. Yasuda, S. Todo, and H. Takayama, Phys. Rev. B **65**, 014407 (2001).
[38] R. Kenna and B. Berche, Condens. Matter Phys. **16**, 23601 (2013).
[39] K. Coester, D. G. Joshi, M. Vojta, and K. P. Schmidt, Phys. Rev. B **94**, 125109 (2016).
[40] W. Zwerger, Phys. Rev. Lett. **92**, 027203 (2004).
[41] D. Podolsky and S. Sachdev, Phys. Rev. B **86**, 054508 (2012).
[42] Y. T. Katan and D. Podolsky, Phys. Rev. B **91**, 075132 (2015).
[43] Y. Q. Qin, B. Normand, A. W. Sandvik, and Z. Y. Meng, following Letter, Phys. Rev. Lett. **118**, 147207 (2017).